Published in final edited form as:
Arch Ophthalmol. 2004 August ; 122(8): 1190–1200. doi:10.1001/archopht.122.8.1190.

Retinal Degeneration in a Rodent Model of Smith-Lemli-Opitz Syndrome:

Electrophysiologic, Biochemical, and Morphologic Features

Steven J. Fliesler, PhD, **Neal S. Peachey, PhD**, **Michael J. Richards, BA**, **Barbara A. Nagel, BA, MS**, and **Dana K. Vaughan, PhD**
From the Departments of Ophthalmology (Dr Fliesler, Mr Richards, and Ms Nagel) and Pharmacological and Physiological Sciences (Dr Fliesler), Saint Louis University School of Medicine, St Louis, Mo; Cleveland Veterans Administration Medical Center (Dr Peachey) and Cole Eye Institute, The Cleveland Clinic Foundation, (Dr Peachey), Cleveland, Ohio; and the Department of Biology, University of Wisconsin–Oshkosh (Dr Vaughan).

Abstract

Objective—To assess the electrophysiologic, histologic, and biochemical features of an animal model of Smith-Lemli-Opitz syndrome (SLOS).

Methods—Sprague-Dawley rats were treated with AY9944, a selective inhibitor of 3β-hydroxysterol-Δ^7-reductase (the affected enzyme in SLOS). Dark- and light-adapted electroretinograms were obtained from treated and control animals. From each animal, 1 retina was analyzed by microscopy, and the contralateral retina plus serum samples were analyzed for sterol composition. The main outcome measures were rod and cone electroretinographic amplitudes and implicit times, outer nuclear layer (ONL) thickness, rod outer segment length, pyknotic ONL nucleus counts, and the 7-dehydrocholesterol/ cholesterol mole ratio in the retina and serum.

Results—By 10 weeks' postnatal age, rod and cone electroretinographic wave amplitudes in AY9944-treated animals were significantly reduced and implicit times were significantly increased relative to controls. Maximal rod photoresponse and gain values were reduced approximately 2-fold in treated animals relative to controls. The ONL thickness and average rod outer segment length were reduced by approximately 18% and 33%, respectively, and ONL pyknotic nucleus counts were approximately 4.5-fold greater in treated animals relative to controls. The retinal pigment epithelium of treated animals contained massive amounts of membranous/lipid inclusions not routinely observed in controls. The 7-dehydrocholesterol/cholesterol mole ratios in treated retinas and serum samples were approximately 5:1 and 9:1, respectively, whereas the ratios in control tissues were essentially zero.

Conclusions—This rodent model exhibits the key biochemical hallmarks associated with SLOS and displays electrophysiologic deficits comparable to or greater than those observed in the human disease.

Correspondence: Steven J. Fliesler, PhD, Department of Ophthalmology, Saint Louis University School of Medicine, 1755 S Grand Blvd, St Louis, MO 63104-1540 (fliesler@slu.edu).

The authors have no relevant financial interest in this article.

This study was presented in part at the Annual Meeting of the Association for Research in Vision and Ophthalmology; May 5–10, 2002; Ft Lauderdale, Fla; the Xth International Symposium on Retinal Degeneration; September 30-October 5, 2002; Burgenstock, Switzerland; the National Institutes of Health (NICDH) Symposium on Inborn Errors of Cholesterol Synthesis; November 14–15 2002; Bethesda, Md; and the Fifth Scientific Symposium on Smith-Lemli-Opitz Syndrome; June 27 2003; Denver, Colo.

Clinical Relevance—These results predict retinal degeneration in patients with SLOS, particularly those with the more severe (type II) form of the disease, and may be more broadly relevant to other inborn errors of cholesterol biosynthesis. This animal model may also be of use in evaluating therapeutic treatments for SLOS and in understanding the slow phototransduction kinetics observed in patients with SLOS.

Smith-Lemli-Opitz syn-drome (SLOS) (OnlineeMendelian Inheritance in Man [OMIM] 270400)1 is the first described example of a "multiple congenital anomalies syndrome" and the first in a growing list of human hereditary diseases involving inborn errors of cholesterol biosynthesis.2–4 This often lethal, autosomal recessive disease affects an estimated 1 in 20000 to 1 in 60000 primarily white live births worldwide, although the incidence may be as high as 1 in 1590 to 1 in 13500 (see Battaile et al5), arguably making it the fourth most prevalent autosomal recessive human disease known. The key biochemical features associated with SLOS are abnormal (typically grossly elevated) levels of 7-dehydro-cholesterol (7DHC), a penultimate precursor of cholesterol, and markedly reduced levels of cholesterol in blood and other bodily tissues.6–9 This abnormality in sterol composition is a consequence of defective activity in the enzyme 3β-hydroxysterol-Δ7-reductase (EC 1.3.1.21), which catalyzes the conversion of 7DHC to cholesterol.10–12 The enzymatic defect, in turn, can be ascribed to any one of a myriad of mutations found to be associated with the *DHCR7* gene (localized to 11q12-q13), which encodes the Δ7-reductase enzyme.13–15 Patients with SLOS exhibit a constellation of profound phenotypic and functional abnormalities, including microcephaly, holoprosencephaly, dysmorphic craniofacial features, micrognathia, limb asymmetries, syndactyly of the second and third toes, polydactyly, ambiguous genitalia, hypospadias, cleft palate, short nose with anteverted nostrils, abnormal visceral development (especially the kidneys, liver, and lungs), hypotonia, failure to thrive, and mental retardation.1–4

Reported ophthalmologic defects associated with SLOS include choroidal hemangiomas, absence of lacrimal puncta, blepharoptosis, pale optic discs, optic atrophy, optic nerve hypoplasia, sclerocornea and corneal endothelium defects, cataracts, and aniridia.16–28 However, these findings were not uniformly observed in all of the relevant published cases and are not conclusive in the differential diagnosis of SLOS. In the single published case of retinal histopathologic features associated with SLOS, based on light and electron microscopic analysis of eyes obtained from a 1-month-old boy, Kretzer et al[23] described extensive retinal ganglion cell and axonal dropout, particularly in the peripheral retina, with incipient optic nerve demyelination, as well as "mitochondrial disintegration" in the retinal pigment epithelium (RPE) and the accumulation of "cytoplasmic masses" in the subretinal space proximal to the photoreceptor outer segments. However, the retina exhibited relatively normal histologic stratification and development, including the presence of grossly normal rod and cone photoreceptor cells.

Animal models for SLOS have been developed by treating rats with selective pharmacologic inhibitors of 3β-hydroxysterol-Δ^7-reductase, such as the experimental drugs AY9944 (*trans*-1,4-*bis* [2-dichlorobenzylamino-ethyl] cyclohexane dihydrochloride)[29–31] and BM15.766.32–35 In addition, a genetic knockout mouse model also has been developed using homologous recombination to delete much of the structural gene encoding the Δ^7-reductase, but the affected progeny live only 18 to 24 hours post partum, thus greatly limiting the utility of this animal model for experimental studies.36,37 We previously described a rat model of SLOS38 created by the dietary treatment of pregnant female rats with AY9944 during the second and third gestational weeks followed by the systemic injection of the progeny with the drug during a 1-month postnatal period. Using this model, we found that despite marked perturbation of cholesterol synthesis, including the gross elevation of 7DHC levels and reduction of cholesterol levels in the blood, retina, liver, and brain, the histologic and ultrastructural development of the retina proceeded normally, and the electrophysiologic

competence of the retina was not substantially compromised. However, in subsequent studies[39] in which postnatal treatment was extended an additional 2 weeks, we observed reduced dark-adapted electroretinographic (ERG) b-wave amplitudes and increased implicit times in AY9944-treated rats, although there were no apparent histologic abnormalities in their retinas. These findings prompted us to speculate that if we extend the treatment period sufficiently, we would observe even more severe ERG deficits and frank histologic degenerative changes. Herein, we provide compelling evidence demonstrating that long-term AY9944 treatment in rats (up to postnatal age 10 weeks) causes profound retinal degeneration, correlating the changes in lipid metabolism with altered cellular physiology and retinal structure. This model mimics the biochemical hallmarks associated with SLOS and is consistent with the recently reported ERG abnormalities associated with this devastating human disease.[40]

METHODS

ANIMALS

Pregnant Sprague-Dawley rats (Harlan Sprague Dawley Inc, Indianapolis, Ind) (received 6 days after fertilization) and their progeny were used. Rats were fed a cholesterol-free chow (Purina Mills TestDiet, Richmond, Ind), with food and water provided ad libitum, and were maintained under dim cyclic lighting (20–40 lux; with a 12-hour light and 12-hour dark cycle) at standard room temperature (22°C-25°C). All procedures were approved by the Saint Louis University Animal Care Committee and were in accordance with the *ARVO Resolution on the Use of Animals in Research* and with the *NIH Guide for the Care and Use of Laboratory Animals*.

AY9944 TREATMENT PROTOCOL

AY9944 was obtained by custom synthesis and purified by re-crystallization to homogeneity (A. H. Fauq, PhD, and S.J.F., unpublished data, 2003), with its chemical, physical, and spectroscopic properties confirmed by comparison with an authentic sample of AY9944 (a gift from Wyeth-Ayerst Research, Princeton, NJ). The treatment protocol was essentially as described previously by Fliesler et al,[38] except the treatment period was extended to 10 postnatal weeks. In brief, pregnant (6 days after fertilization) Sprague-Dawley rats were fed cholesterol-free chow containing AY9944 (1 mg/100 g of chow; maximum of 40 g of chow daily) for the last 2 weeks of the 3-week gestational period. Progeny were then injected on alternating days, 3 times per week, with an aqueous olive oil emulsion containing AY9944 (10 mg/mL; 25–30 mg/kg of body weight) and with a mixture of the fat-soluble vitamins A, D, and E. Controls were injected with vehicle alone and also were fed cholesterol-free chow.

ELECTRORETINOGRAPHY

The ERGs were recorded from 4 control rats and 5 AY9944-treated rats. Animals were dark adapted overnight and then anesthetized by intramuscular injection of ketamine hydrochloride (75 mg/kg) and xylazine hydrochloride (5 mg/kg). The pupils were dilated with 1% tropicamide and 2.5% phenylephrine hydrochloride, and the rats were placed on a regulated heating pad throughout the recording session. Strobe flash stimuli were presented using a Ganzfeld bowl (LKC Technologies, Gaithersburg, Md). The ERGs were recorded from both eyes using a thin stainless steel wire contacting the corneal surface through a thin layer of 1% methylcellulose. Platinum needle electrodes inserted into the cheek below each eye and into the tail served as reference and ground leads, respectively. Responses were differentially amplified (0.5–1500 Hz), averaged, and stored using a signal-averaging system (model UTAS E-2000; LKC Technologies).

In each recording session, a dark-adapted response series was obtained first using strobe flash stimuli that ranged in intensity from −4.3 to 0.5 log candela (cd)-sec/m^2, controlled by placing Wratten neutral density filters (Eastman Kodak Co, Rochester, NY) in the light path. Stimuli were presented in order of increasing intensity, and at least 2 responses were averaged at each flash intensity. A steady rod-desensitizing adapting field (0.6 cd/m^2) was then presented in the Ganzfeld bowl. After 7 minutes of light adaptation, responses were recorded to strobe stimuli ranging from 1.2 to 0.5 log cd-sec/m^2. At each intensity, responses to 50 successive flashes presented at 2.1 Hz were averaged.

The a-wave amplitude was measured from the prestimulus baseline to the trough of the a-wave, whereas the b-wave was measured to the positive peak, either from the trough of the a-wave or (if no a-wave was present) from the baseline. Implicit times for a- and b-waves were measured from the time of stimulus presentation to the a-wave trough and to the b-wave peak, respectively.

We also analyzed the leading edge of the dark-adapted a-wave in terms of a modified form of the Lamb and Pugh model of rod phototransduction[41,42]:

$$P3(i,t) = \{1 - exp[-iS(t - t_d)2]\}\ R_{mP3},$$

where *P3* represents the mass response of the rod photoreceptors, the amplitude of which is expressed as a function of flash energy (*i*) and time (*t*) after flash onset; *S*, the gain of phototransduction; R_{mP3}, the maximum response; and t_d, a brief delay. This model was initially applied to human control and patient data,[43,44] and it has been used since to model the leading edge of the rodent a-wave.[45–47] Application of this model requires the use of high-intensity stimuli.[40] Owing to this constraint, we only fit the model to responses obtained to the highest-intensity stimulus (0.5 log cd-sec/m^2). To provide a basis of comparison with data reported by Elias et al[40] from patients with SLOS, we converted 0.5 log cd-sec/m^2 to 16520 R* using a conversion factor of 1 cd-sec/m^2 approximately equal to 5012 R*, where R* represents the number of rhodopsin photoisomerization events per rod.

LIPID ANALYSIS

Methods used for the saponification, extraction, chromatographic resolution (reverse-phase high-performance liquid chromatography), identification, and quantitative measurement of sterols from rat tissues (including serum, neural retina, liver, and brain) were as described in detail elsewhere.38,48 All procedures were performed under dim room illumination to minimize light-induced isomerization and degradation of lipids. Tissue samples were harvested immediately after ERG recording, while the animals were still under deep anesthesia. Blood samples were obtained by intracardiac puncture, and serum samples were prepared by centrifugation of whole blood after allowing for clotting to occur. One eye from each animal was harvested for histologic and ultrastructural analysis (see the following subsection); neural retinas (free of RPE) from contralateral eyes were rapidly dissected out and snap frozen in liquid nitrogen, as were the livers, brains, and serum samples. Specimens were stored in darkness at −85°C until ready for analysis. Immediately before saponification, tissues were supplemented with an internal standard of [^{3}H] cholesterol (American Radiolabeled Chemicals Inc, St Louis, Mo) to provide a means of correcting for losses incurred during preparation of the nonsaponifiable lipid extracts and to act as an internal chromatographic standard for comparison with the mass elution profiles (UV detection, 205 nm). Identification and quantification of sterols and sterol mass were accomplished by comparing the individual chromatographic peak retention times and integrated peak areas with those of authentic sterol standards, particularly cholesterol and 7DHC (obtained from Sigma-Aldrich Corp, St Louis; recrystallized from methanol-water twice before use). In addition, the chromatographic

properties and detector response factor (high-performance liquid chromatography integration units per nanomole of sterol) were determined for an authentic standard of 8-dehydrocholesterol (8DHC) (cholesta-5,8[9]-dien-3β-ol), obtained previously as a gift from George J. Schroepfer, Jr, MD, PhD (Rice University, Houston, Tex).

HISTOLOGIC AND ULTRASTRUCTURAL ANALYSIS

Retinas from the eyes of AY9944-treated and control rats were analyzed at the light and electron microscope levels essentially as described in a previous publication.[49,50] In brief, 1 eye each from treated and control animals was immersed over-night at 4°C in buffered mixed aldehyde fixative (2% glutaraldehyde, 2% paraformaldehyde, in 0.125M sodium cacodylate buffer, pH 7.4, containing 0.025% calcium chloride), after removal of the superior cornea and the lens; the inferior cornea was left in place to serve as a geographic marker. After buffer rinses, osmification, and dehydration through a graded ethanol series, eyes were embedded in epoxy resin (Spurrs formulation), and 0.75-μm-thick sections were collected onto glass microscope slides using an ultramicrotome (UltraCut-E; Reichert Ophthalmic Instruments, Depew, NY). Eyes were sectioned along the vertical meridian through the optic nerve head, from the superior ora serrata to the inferior ora serrata, and examined by light microscopy after staining with 1% toluidine blue and coverslipping using a photomicroscope (model BH-2; Olympus, Melville, NY) with an oil-immersion lens (20× DPlan-Apo or 60× SPlanApo; Olympus). Digitized images were obtained using a digital camera (model DXM1200; Nikon Instruments Inc, Melville, NY), and images were stored using Nikon software on an IBM-compatible personal computer. Thin (70- to 80-nm) sections corresponding to retinal regions of particular interest were collected onto copper mesh grids, counter-stained with uranyl acetate–lead citrate, and examined using an electron microscope (model 100CX; JEOL USA, Peabody, Mass) and an accelerating voltage of 60 keV.

QUANTITATIVE MORPHOMETRIC ANALYSIS

Quantitative measurements of outer nuclear layer (ONL) thickness, rod outer segment (ROS) lengths, and pyknotic nuclei in the ONL were performed essentially as described previously.[51,52] Resin-embedded blocks of hemisected eyes were sectioned for light microscopy along the vertical meridian, as indicated in the previous subsection. Three serial sections were cut and mounted from each block and then examined and the section plane was adjusted, as needed, for proper ROS alignment. From each section, digitized images were collected at 0.5-mm intervals, beginning at the optic nerve head and proceeding to the far periphery in the inferior and superior hemispheres. From each such image, 5 ONL thickness measurements and 10 ROS length measurements were gathered from random locations within the field of view, and the data were tabulated using a electronic spreadsheet (Excel; Microsoft Corp, Redmond, Wash). This provided 15 independent ONL measurements and 30 independent ROS measurements per locus; mean±SD values for each locus were calculated from eyes obtained from 3 to 5 rats per treatment group and plotted as a function of distance from the optic nerve head, thereby generating a morphometric profile for ONL thickness and ROS length across the vertical meridian for control and treated animals. Summary data averaged across the vertical meridian were further analyzed using a homoscedastic *t* test (Excel); significance was determined at the 95% confidence interval or higher. Using the same fields, pyknotic nuclei in the ONL were counted and recorded. Pyknotic cell counts were summed and tabulated for each linear millimeter of vertical meridian length, and the resulting data were subjected to the same statistical analysis as used for ONL thickness and ROS length measurements.

RESULTS

AY9944 TREATMENT AFFECTS ROD AND CONE FUNCTION

Figure 1A presents a series of representative dark-adapted ERGs obtained from a control rat and a rat treated with AY9944. In each series, the responses to 5 different stimulus intensities are superimposed. Responses obtained from AY9944-treated rats were similar in overall waveform but were smaller in amplitude compared with those from control rats. Figure 1B compares average intensity-response functions for a- and b-wave amplitudes. The responses of AY9944-treated rats were significantly reduced in amplitude below control levels for the a- ($F_{1,7}$=41.5; P<.01) and the b-waves ($F_{1,7}$=12.3; P<.01). Across the stimulus-response range tested, mean±SD a-wave amplitudes of AY9944-treated rats were reduced to 66.9%±15.5% of control values, and b-wave amplitudes were reduced to 81.5% ± 3.1% of control values across the stimulus-intensity range. Figure 1C presents the corresponding implicit time data. The implicit times for rod responses were substantially greater in the treated group than in controls, and these differences were statistically significant for the a- ($F_{1,7}$=28.4; P<.01) and b-waves ($F_{1,7}$=78.1; P<.01). These results indicate a significant perturbation of the rod-localized phototransduction process (reflected in the a-wave) and the bipolar cell response (mirrored by the b-waves).

To further evaluate the effects of AY9944 treatment on rod photoreceptor function, we analyzed the leading edge of the a-wave in terms of the Lamb and Pugh model[41,42] of rod phototransduction. Figure 2A compares the leading edge of the a-wave from each rat in response to the highest-intensity stimulus (0.5 log cd-sec/m^2). In this format, responses have been normalized by dividing the entire response by the maximal response amplitude (R_{mP3}) variable. The leading edge of the a-wave reached the trough more slowly for AY9944-treated rats than for control animals, and there was no overlap between the 2 groups. Figure 2B displays the R_{mP3} values obtained for each rat. The average value of R_{mP3} for the AY9944-treated animals was reduced nearly 2-fold compared with that of controls (t_7=9.8; P<.001). Figure 2C plots the corresponding values of photoreceptor gain (S). The average value of S for the AY9944-treated rats also was reduced nearly 2-fold compared with that of controls (t_7=5.9; P<.001).

Figure 3A compares cone ERGs obtained from a representative control rat and an AY9944-treated rat. The overall amplitude of the cone ERG is reduced after AY9944 treatment. Figure 3B compares average intensity-response functions for cone ERG b-wave amplitude; the responses of AY9944-treated rats were significantly reduced below control levels ($F_{1,7}$=24.8; P<.01). Across the stimulus-response range tested, mean±SD cone ERG amplitudes of AY9944-treated rats were reduced to 60.8%±1.0% of control values. Figure 3C presents the corresponding implicit times, which were significantly prolonged in the treated group compared with controls ($F_{1,7}$=78.1;P<.01). These results indicate that cone photoreceptor function also was markedly affected by AY9944 treatment, as was the function of the depolarizing class of cone bipolar cell, which makes a large contribution to the rat cone ERG under these stimulus and recording conditions.[53]

These findings demonstrate that rod and cone function are markedly affected by prolonged systemic treatment of rats with AY9944. Furthermore, they suggest that visual information processing in the inner retina, at least at the level of bipolar cell function, also is compromised by this treatment.

STEROL COMPOSITION OF RETINA AND OTHER TISSUES IS MARKEDLY AFFECTED BY AY9944 TREATMENT

In good agreement with a previous study,[38] and consistent with results obtained by other researchers[29,31,54–56] regarding the effects of AY9944 on lipid metabolism, rats treated systemically with AY9944 for nearly 3 months exhibited grossly deranged sterol metabolism (Table and Figure 4). This finding is evidenced by the marked accumulation of 7DHC (and lesser amounts of the 8-dehydro isomer, 8DHC) and the substantial reduction in the cholesterol content of retina and serum relative to age-matched controls. In controls, cholesterol is the over-whelmingly dominant, if not exclusive, sterol present in all tissues examined, and steady-state levels of 7DHC and 8DHC are barely detectable, if present at all. In fact, 7DHC was the dominant sterol detected in tissues from AY9944-treated animals, with the 7DHC-cholesterol mole ratio being approximately 5:1 for retinas and nearly 9:1 for serum samples. A similar trend in sterol composition was observed on analysis of whole brain and liver (data not shown). Although 7DHC is, by far, the predominant sterol in the retinas and serum samples of AY9944-treated rats, accumulation of 8DHC also was substantial, with the 8DHC-cholesterol mole ratio for retina being about 0.6 and the 7DHC-8DHC mole ratio being approximately 8.7. On a per retina basis, the total sterol content of retinas from AY9944-treated rats was approximately 80% that of age-matched controls, the difference being largely due to differences in eye size and, hence, overall retinal mass, since treated animals were considerably smaller than controls (eg, only approximately 50%-60% of control body weight). The 7DHC-cholesterol mole ratio for serum samples from AY9944-treated rats also was approximately 8.7, cholesterol levels were reduced to approximately 23% of control levels, and total serum sterol levels also were markedly reduced (by approximately 75%) relative to controls. These latter findings are consistent with the well-known hypolipidemic effects of AY9944.[29–31, 54–56]

AY9944 TREATMENT CAUSES PROGRESSIVE RETINAL DEGENERATION

In contrast to the previously reported lack of histologic alterations induced in rat retinas up to 1 postnatal month of treatment with AY9944,[38] extending the treatment duration up to 3 postnatal months (10 weeks) resulted in obvious histologic changes consistent with progressive retinal degeneration (Figure 5). These changes, which included reduction in ONL thickness, pyknosis of ONL nuclei, dropout of photoreceptor cells, and reduction in ROS length, were observed in the superior (Figure 5A and B) and inferior hemispheres (Figure 5C and D) along the vertical meridian and are in general agreement with the noted reductions in ERG amplitudes. The changes observed in ONL thickness and nuclear pyknosis (measurements relevant to overall photoreceptor viability) as a consequence of extended AY9944 treatment were quantified (Figure 6). Overall, ONL thickness was reduced by approximately 18% relative to controls ($P<.01$), from the optic nerve head region to the periphery, consistent with a loss of approximately 2 of 10 rows of photoreceptor nuclei. Photoreceptor loss was symmetrical, with a comparable degree of ONL thickness reduction observed in the superior and inferior hemispheres. Pyknotic nucleus counts (measured per linear millimeter of retinal expanse along the vertical meridian) in each retinal region examined were consistently and substantially higher (approximately 4.5-fold, on average) in AY9944-treated animals compared with controls, consistent with enhancement of photoreceptor cell death and dropout in AY9944-treated rats.

Superimposed on the loss of photoreceptor cells was a substantial reduction in ROS length in the remnant photoreceptors. Analysis of well-aligned rods in the superior hemisphere revealed an overall 33% loss in ROS length when AY9944-treated rats were compared with controls (mean±SD ROS length, 22.1±3.7 μm and 33.2±2.7 μm, respectively) (Figure 7). A similar reduction in ROS length also was observed in the inferior hemisphere (data not shown); hence, the retinal degeneration seems to be relatively symmetrical and uniform in both hemispheres rather than exhibiting a geographic preference for a particular retinal region. In most other

respects, however, the remnant photoreceptors and their outer segments seemed histologically and ultrastructurally normal (see also the "Comment" section), except for the increased incidence of ONL pyknosis mentioned previously herein. Owing to the relative paucity of identifiable cone photoreceptors in the roddominant rat retina and the difficulties in obtaining optimal cone outer segment alignment from region to region along the vertical meridian, a similar analysis of cone outer segment lengths was not performed.

AY9944 TREATMENT CAUSES MARKED ULTRASTRUCTURAL CHANGES IN THE RPE

In addition to the observed histologic changes in the neural retina, examination at the ultrastructural level revealed that the RPE in AY9944-treated rats was abnormal compared with that in age-matched controls (Figure 8). The RPE cytoplasm in treated rats was congested with numerous membranous and osmophilic (presumed lipid-laden) inclusions, including phagosomes, multivesicular bodies, and residual bodies, well beyond the normal level of such inclusions in the RPE of control rats. Again, this pathological feature did not exhibit any apparent regional preference but was consistently observed along the entire vertical meridian in the superior and inferior hemispheres.

In addition, unlike in control rats, where the RPE exhibited an accumulation and then clearance of ingested ROS tips (phagosomes) as a function of the time of day,[57,58] the congestion of the RPE in AY9944-treated rats seemed relatively invariant throughout the day (data not shown). Regardless, the RPE in treated rats maintained its normal polarity, for example, distribution of mitochondria proximal to the basal plasmalemma and the Bruch membrane, extension of apical microvilli, and maintenance of basolateral membrane and junctional complex integrity. Also, at this stage of treatment, there was no evidence of appreciable RPE hypertrophy or hyperplasia, RPE nuclear chromatin appeared comparable to that of controls, there was no obvious change in the thickness of the Bruch membrane, and there was no apparent increased deposition of lipid inclusions in the Bruch membrane relative to controls.

COMMENT

We described the electrophysiologic (ERG), biochemical, histologic, and ultrastructural features of a progressive retinal degeneration in a rodent model of SLOS. The deficits in photoreceptor-mediated retinal function are generally consistent with the observed photoreceptor degeneration, as characterized by a reduction in the ROS length with increased photoreceptor pyknosis and cell loss (ie, diminished ONL thickness). The definitive biochemical features of this animal model—an elevated 7DHC-cholesterol mole ratio (due to high 7DHC levels and low cholesterol levels) and a marked reduction in total serum sterol levels relative to controls—are consistent with the hallmarks of the human hereditary disease, particularly as observed in the more severe (type II) form of SLOS.[1–4,6–11] However, a direct comparison between the retinal histopathologic features of our animal model and those of human SLOS must await analysis of a larger cohort of SLOS donor eyes than currently exists.

As mentioned previously herein, the only published description of SLOS retinal histopathologic features is that provided by Kretzer et al[23] in a case report of an ocular specimen obtained from an affected 1-month-old boy. The neurosensory retina exhibited relatively normal histologic stratification of the cellular layers and well-differentiated rods and cones. Those findings are consistent with our previous study[38] of the AY9944-induced SLOS animal model, where the retina appeared relatively normal, histologically and ultrastructurally, in the first postnatal month of life.

Atchaneeyasakul et al[28] described variable ocular findings in a group of 8 children (aged 1 week to 5 years) with well-documented SLOS ranging from mild to moderately severe disease phenotypes. In addition, the sterol composition of ocular tissues (including the neural retina,

RPE, lens, cornea, sclera, and ocular muscle) from a spontaneously aborted fetus (32 weeks' gestation) affected with SLOS was reported in that study, with the corresponding tissues from the eyes of a nonaffected 3-month-old child serving as a control. All ocular tissues from the fetus with SLOS exhibited grossly elevated levels of 7- and 8-dehydrosterols compared with normal eyes (which did not exhibit any detectable 7DHC or 8DHC), with 7DHC-cholesterol mole ratios ranging from approximately 0.4 for the retina, cornea, sclera, and muscle to 1.48 for the lens, with the ratio for the RPE being 0.93. Qualitatively, these results are consistent with the biochemical findings in our animal model, although our animals exhibited more profoundly deranged cholesterol biosynthesis.

The recent study by Elias et al,40 which represents the first ERG study of patients with SLOS, demonstrates significantly delayed rod activation and deactivation kinetics, as well as reduced postreceptor sensitivities, compared with unaffected controls. In that study, the sensitivity variable S (see Hood and Birch44) for patients with SLOS was found to be only approximately 61% of the value determined for controls. This variable reflects relative mobilities of and efficiency of interactions between the components of the phototransduction cascade, from initial photon absorption by the visual pigment rhodopsin to the closing of the cyclic guanosine monophosphate–gated ion channels in the outer segment plasma membrane that govern the "dark current" in the rod cell.42 Those findings are consistent with the ones reported in the present study since we observed an approximately 2-fold decrease in the value of S in retinas from AY9944-treated rats compared with controls. Elias et al40 hypothesized that the presumed decrease in cholesterol content of the ROS membranes, as inferred from the known inhibition of cholesterol biosynthesis and from the blood sterol analysis of their patients, may explain the slow phototransduction kinetics. However, we consider this unlikely given that (1) ROS membranes are notably cholesterol deficient naturally relative to other mammalian plasma membranes59 and, (2) if anything, a decrease in the cholesterol content of the membrane would be expected to increase the lateral mobility of the constituent membrane proteins, thereby increasing their interactions and, concomitantly, enhancing the rate of phototransduction because cholesterol tends to restrict molecular motions (decrease membrane fluidity) above the phase transition temperature of the membrane lipids.60›61 At this point, the reason for the slow kinetics of phototransduction remains unclear. However, the experimental model described herein offers the ability to examine structure-function relationships in a systematic manner, with the potential of answering this question.

In contrast to the findings of Elias et al,[40] where patients with SLOS were found to have, on average, only a slight decrease (approximately 16%) in the saturated amplitude of the rod response (R_{mP3}), our SLOS rat model exhibited nearly a 2-fold reduction in the average R_{mP3} value relative to controls. The profound reduction in rod responses in the AY9944-treated rat may be due, in part, to the loss of nearly one third of the length of the ROS and the nearly 20% reduction in the total number of remaining viable rods. Because there was no correlative assessment of retinal histologic characteristics in the study by Elias et al,[40] and, to our knowledge, there are no age-matched SLOS retinal histologic specimens reported in the literature, further direct comparisons between our experimental animal study and the recently reported study of human patients with SLOS cannot be made.

In addition to a-wave abnormalities, the timing of dark-adapted b-waves of AY9944-treated rats was significantly slower than in control rats. Although the b-wave represents the mass response of rod bipolar cells62 and is thus affected by changes at the photoreceptor level, a computational model of the ERG (see Hood and Birch63) indicates that the implicit time changes noted here cannot be replicated by a decrease in either S or R_{mP3}. Both of these changes will shift the implicit time function to the right along the stimulus-intensity axis but will not cause delays at low stimulus intensities. Instead, these results indicate that there is an additional defect at the level of b-wave generation, at the synaptic level, or in bipolar cell signal

transduction. Cone dysfunction associated with SLOS was not evaluated in the study by Elias et al[40] or in any other published study, to our knowledge. In the present study, we showed that light-adapted ERGs of AY9944-treated rats are dramatically altered compared with those of normal rats, that the average maximum cone response amplitude was reduced by at least 40%, and that implicit times were substantially increased. Assuming that the rat model mimics the human disease, these results would predict that patients with SLOS would exhibit cone dysfunction as well as the previously documented rod dysfunction.

Why should derangement of cholesterol biosynthesis, with concomitant accumulation of 7DHC, cause photoreceptor cell death and retinal degeneration? In brief, it has been proposed that cytotoxic "oxysterols" derived from 7DHC may be involved (for a detailed discussion, see Fliesler64). Hence, this may represent yet another (albeit somewhat specialized) example of the lipid peroxidation mechanisms that have been implicated in the pathobiologic features of retinal degenerations, including experimental retinal light damage,[65–67] age-related macular degeneration,[67–69] and uveitis.[70] This hypothesis is supported further by a series of studies in our laboratory that have shown that (1) SLOS rats are markedly more susceptible to retinal light damage than are normal albino rats,[39] (2) treatment of SLOS rats with a systemic antioxidant before intense light exposure can protect against retinal light damage,[71] and (3) steady-state levels of lipid hydroperoxides in the retinas of SLOS rats are approximately 2-fold higher than those in controls, and exposure to retinal light damage conditions produces an additional 3-fold elevation in retinal lipid hydroperoxides, with concomitantly greater histologic damage than observed in light-exposed normal rats.[72] In addition, cholesta-5,7,9(11)-trien-3β-ol (a compound generated by the decomposition of 7-hydroperoxy-cholesta-5,8-dien-3β-ol, a sterol hydroperoxide formed by the photo-oxidation of 7DHC) has been identified in the plasma of patients with SLOS.[73] Furthermore, by-products of 7DHC oxidation have been shown to retard the growth rate of cultured rat embryos, a fact that may have particular significance with respect to the in utero developmental abnormalities associated with SLOS.[74]

Regarding the ultrastructural abnormalities observed in the RPE of rats treated with AY9944, we speculate that the observed accumulation of membranous inclusions and lipid deposits may be due to inhibition of lysosomal enzymes requisite for phagosome digestion. Consistent with this finding, Sakuragawa et al[75] described a Niemann-Pick rodent model produced by AY9944 administration, with "lamellar inclusion bodies" appearing in the retina, lens, and other ocular and nonocular tissues, including glia and neurons in the brain. Although the mechanism underlying these observations is speculative and has been challenged by subsequent studies,[76,77] to our knowledge, the possibility that oxysterols derived from 7DHC are involved, either primarily or secondarily, has not been proposed or examined by other researchers. Studies are currently under way in our laboratory to test this hypothesis directly.

Finally, in addition to offering an experimentally accessible system to study the mechanisms underlying the retinal degeneration and electrophysiologic dysfunction associated with SLOS, this animal model provides a valuable tool for examining possible therapeutic interventions, such as dietary cholesterol supplementation. This may allow further design optimization of therapeutic conditions (eg, combined cholesterol-antioxidant regimens) to be used in clinical treatment trials in addition to those currently in progress.[27,78–81]

Acknowledgments

This study was supported in part by grant EY07361 from the US Public Health Service, Washington, DC (Dr Fliesler); by an unrestricted departmental grant from Research to Prevent Blindness, New York, NY (Dr Fliesler); and by funding from the Department of Veteran Affairs, Washington, DC (Dr Peachey).

We thank Ellen R. Elias, MD, Anne B. Fulton, MD, and Ronald M. Hansen, PhD, for helpful discussions and for providing the results of their ERG study of patients with SLOS before publication.

REFERENCES

1. Smith JD, Lemli L, Opitz JM. A newly recognized syndrome of multiple congenital anomalies. J Pediatr 1964;64:210–217. [PubMed: 14119520]
2. Kelley RI. Inborn errors of cholesterol biosynthesis. Adv Pediatr 2000;47:1–53. [PubMed: 10959439]
3. Porter FD. Human malformation syndromes due to inborn errors of cholesterol synthesis. Curr Opin Pediatr 2003;15:607–613. [PubMed: 14631207]
4. Herman GE. Disorders of cholesterol biosynthesis: prototypic metabolic malformation syndromes. Hum Mol Genet 2003;12:R75–R88. [PubMed: 12668600]
5. Battaile KP, Battaile BC, Merkens LS, Maslen CL, Steiner RD. Carrier frequency of the common mutation IVS8-1G>C in DHCR7 and estimate of the expected incidence of Smith-Lemli-Opitz syndrome. Mol Genet Metab 2001;72:67–71. [PubMed: 11161831]
6. Irons M, Elias ER, Salen G, Tin S, Batta AK. Defective cholesterol biosynthesis in Smith-Lemli-Opitz syndrome [letter]. Lancet 1993;341:1414. [PubMed: 7684480]
7. Tint GS, Irons M, Elias ER, et al. Defective cholesterol biosynthesis associated with the Smith-Lemli-Opitz syndrome. N Engl J Med 1994;330:107–113. [PubMed: 8259166]
8. Cunniff C, Kratz LE, Moser A, Natowicz MR, Kelley RI. Clinical and biochemical spectrum of patients with RSH/Smith-Lemli-Opitz syndrome and abnormal cholesterol metabolism. Am J Med Genet 1997;68:263–269. [PubMed: 9024557]
9. Yu H, Lee MH, Starck L, et al. Spectrum of Δ7-dehydrocholesterol reductase mutations in patients with the Smith-Lemli-Opitz (RSH) syndrome. Hum Mol Genet 2000;9:1385–1391. [PubMed: 10814720]
10. Salen G, Shefer S, Batta AK, et al. Abnormal cholesterol biosynthesis in the Smith-Lemli-Opitz syndrome. J Lipid Res 1996;37:1169–1180. [PubMed: 8808751]
11. Tint GS, Batta AK, Xu G, et al. The Smith-Lemli-Opitz syndrome: a potentially fatal birth defect caused by a block in the last enzymatic step in cholesterol biosynthesis. Subcell Biochem 1997;28:117–144. [PubMed: 9090293]
12. Waterham HR, Wanders RJ. Biochemical and genetic aspects of 7-dehydrocholesterol reductase and Smith-Lemli-Opitz syndrome. Biochim Biophys Acta 2000;1529:340–356. [PubMed: 11111101]
13. Witsch-Baumgartner M, Fitzky BU, Ogorelkova M, et al. Mutational spectrum in the Δ7-sterol reductase gene and genotype-phenotype correlation in 84 patients with Smith-Lemli-Opitz syndrome. Am J Hum Genet 2000;66:402–412. [PubMed: 10677299]
14. Nowaczyk MJ, Nakamura LM, Waye JS. DHCR7 and Smith-Lemli-Opitz syndrome. Clin Invest Med 2001;24:311–317. [PubMed: 11767235]
15. Jira PE, Waterham HR, Wanders RJ, Smeitink JA, Sengers RC, Wevers RA. Smith-Lemli-Opitz syndrome and the DHCR7 gene. Ann Hum Genet 2003;67(pt 3):269–280. [PubMed: 12914579]
16. Finley SC, Finley WH, Monsky DB. Cataracts in a girl with features of the Smith-Lemli-Opitz syndrome. J Pediatr 1969;75:706–707. [PubMed: 5809847]
17. Cotlier E, Rice P. Cataracts in the Smith-Lemli-Opitz syndrome. Am J Ophthalmol 1971;72:955–959. [PubMed: 4330375]
18. Gold JD, Pfafffenbach DD. Ocular abnormalities in the Smith-Lemli-Opitz syndrome. J Pediatr Ophthalmol 1975;12:228–234.
19. Gracia R, Nieto JA, Nistal M, et al. Aniridia associated with gonadoblastoma in Smith-Lemli-Opitz syndrome (author's transl) [in Spanish]. An Esp Pediatr 1976;9:19–24. [PubMed: 1015678]
20. Fierro M, Martinez AJ, Harbison JW, Hay SH. Smith-Lemli-Opitz syndrome: neuropathological and ophthalmological observations. Dev Med Child Neurol 1977;19:57–62. [PubMed: 844667]
21. Harbin RL, Katz JI, Frias JL, Rabinowicz IM, Kaufman HE. Sclerocornea associated with the Smith-Lemli-Opitz syndrome. Am J Ophthalmol 1977;84:72–73. [PubMed: 900220]
22. Freedman RA, Baum JL. Postlenticular membrane associated with Smith-Lemli-Opitz syndrome. Am J Ophthalmol 1979;87:675–677. [PubMed: 443339]

23. Kretzer FL, Hittner HM, Mehta RS. Ocular manifestations of the Smith-Lemli-Opitz syndrome. Arch Ophthalmol 1981;99:2000–2006. [PubMed: 7295150]
24. Bardelli AM, Lasorella G, Barberi L, Vanni M. Ocular manifestations in Kniest syndrome, Smith-Lemli-Opitz syndrome, Hallermann-Streiff-Francois syndrome, Rubinstein-Taybi syndrome and median cleft face syndrome. Ophthalmic Paediatr Genet 1985;6:343–347. [PubMed: 3934624]
25. Belmont JW, Hawkins E, Hejtmancik JF, Greenberg F. Two cases of severe lethal Smith-Lemli-Opitz syndrome. Am J Med Genet 1987;26:65–67. [PubMed: 3812579]
26. Curry CJ, Carey JC, Holland JS, et al. Smith-Lemli-Opitz syndrome-type II: multiple congenital anomalies with male pseudohermaphroditism and frequent early lethality. Am J Med Genet 1987;26:45–57. [PubMed: 3812577]
27. Elias ER, Irons MB, Hurley AD, Tint GS, Salen G. Clinical effects of cholesterol supplementation in six patients with the Smith-Lemli-Opitz syndrome (SLOS). Am J Med Genet 1997;68:305–310. [PubMed: 9024564]
28. Atchaneeyasakul LO, Linck LM, Connor WE, Weleber RG, Steiner RD. Eye findings in 8 children and a spontaneously aborted fetus with RSH/Smith-Lemli-Opitz syndrome. Am J Med Genet 1998;80:501–505. [PubMed: 9880216]
29. Kolf-Clauw M, Chevy F, Wolf C, Siliart B, Citadelle D, Roux C. Inhibition of 7-de-hydrocholesterol reductase by the teratogen AY9944: a rat model for Smith-Lemli-Opitz syndrome. Teratology 1996;54:115–125. [PubMed: 8987154]
30. Kolf-Clauw M, Chevy F, Ponsart C. Abnormal cholesterol biosynthesis as in Smith-Lemli-Opitz syndrome disrupts normal skeletal development in the rat. J Lab Clin Med 1998;131:222–227. [PubMed: 9523845]
31. Chambers CM, McLean MP, Ness GC. Smith-Lemli-Opitz syndrome produced in rats with AY 9944 treated by intravenous injection of lipoprotein cholesterol. Am J Med Genet 1997;68:322–327. [PubMed: 9024567]
32. Xu G, Salen G, Shefer S, et al. Treatment of the cholesterol biosynthetic defect in Smith-Lemli-Opitz syndrome reproduced in rats by BM 15.766. Gastroenterology 1995;109:1301–1307. [PubMed: 7557099]
33. Wolf C, Chevy F, Pham J, et al. Changes in serum sterols of rats treated with 7-dehydrocholesterol-Δ7-reductase inhibitors: comparison to levels in humans with Smith-Lemli-Opitz syndrome. J Lipid Res 1996;37:1325–1333. [PubMed: 8808767]
34. Kolf-Clauw M, Chevy F, Siliart B, Wolf C, Mulliez N, Roux C. Cholesterol biosynthesis inhibited by BM 15.766 induces holoprosencephaly in the rat. Teratology 1997;56:188–200. [PubMed: 9358606]
35. O'Brien WT, Xu G, Tint GS, Salen G, Servatius RJ. Blocking cholesterol synthesis impairs acquisition of the classically conditioned eyeblink response. Integr Physiol Behav Sci 2000;35:120–131. [PubMed: 11021337]
36. Fitzky BU, Moebius FF, Asaoka H, et al. 7-Dehydrocholesterol-dependent proteolysis of HMG-CoA reductase suppresses sterol biosynthesis in a mouse model of Smith-Lemli-Opitz/RSH syndrome. J Clin Invest 2001;108:905–915. [PubMed: 11560960]
37. Wassif CA, Zhu P, Kratz L, et al. Biochemical, phenotypic and neurophysiological characterization of a genetic mouse model of RSH/Smith-Lemli-Opitz syndrome. Hum Mol Genet 2001;10:555–564. [PubMed: 11230174]
38. Fliesler SJ, Richards MJ, Miller CY, Peachey NS. Marked alteration of sterol metabolism and composition without compromising retinal development or function. Invest Ophthalmol Vis Sci 1999;40:1792–1801. [PubMed: 10393050]
39. Fliesler SJ, Richards MJ, Peachey NS, Buchan B, Vaughan DK, Organisciak DT. Potentiation of retinal light damage in an animal model of Smith-Lemli-Opitz syndrome [ARVO abstract]. Invest Ophthalmol Vis Sci 2001;42:S627. Abstract 3373.
40. Elias ER, Hansen RM, Irons M, Quinn NB, Fulton AB. Rod photoreceptor responses in children with Smith-Lemli-Opitz syndrome. Arch Ophthalmol 2003;121:1738–1743. [PubMed: 14662594]
41. Lamb TD, Pugh EN Jr. A quantitative account of the activation steps involved in phototransduction in amphibian photoreceptors. J Physiol 1992;449:719–758. [PubMed: 1326052]

42. Pugh EN Jr, Lamb TD. Amplification and kinetics of the activation steps in phototransduction. Biochim Biophys Acta 1993;1141:111–149. [PubMed: 8382952]
43. Breton ME, Schueller AW, Lamb TD, Pugh EN Jr. Analysis of ERG a-wave amplification and kinetics in terms of the G-protein cascade of phototransduction. Invest Ophthalmol Vis Sci 1994;35:295–309. [PubMed: 8300357]
44. Hood DC, Birch DG. Rod phototransduction in retinitis pigmentosa: estimation and interpretation of parameters derived from the rod a-wave. Invest Ophthalmol Vis Sci 1994;35:2948–2961. [PubMed: 8206712]
45. Goto Y, Peachey NS, Ziroli NE, et al. Rod phototransduction in transgenic mice expressing a mutant opsin gene. J Opt Soc Am A 1996;13:577–585.
46. Lyubarsky AL, Pugh EN Jr. Recovery phase of the murine rod photoresponse reconstructed from electroretinographic recordings. J Neurosci 1996;16:563–571. [PubMed: 8551340]
47. Cheng T, Peachey NS, Li S, Goto Y, Cao Y, Naash MI. The effect of peripherin/ rds haploinsufficiency on rod and cone photoreceptors. J Neurosci 1997;17:8118–8128. [PubMed: 9334387]
48. Fliesler SJ, Richards MJ, Miller C, Peachey NS, Cenedella RJ. Retinal structure and function in an animal model that replicates the biochemical hallmarks of desmosterolosis. Neurochem Res 2000;25:685–694. [PubMed: 10905631]
49. Pittler SJ, Fliesler SJ, Fisher P, Keller RK, Rapp LM. In vivo requirement of protein prenylation for maintenance of retinal cytoarchitecture and photoreceptor structure. J Cell Biol 1995;130:1–9. [PubMed: 7540613]
50. Fliesler SJ, Richards MJ, Miller CY, Cenedella RJ. Cholesterol synthesis in the vertebrate retina: effects of U18666A on rat retinal structure, photoreceptor membrane assembly, and sterol metabolism and composition. Lipids 2000;35:289–296. [PubMed: 10783006]
51. Vaughan DK, Nemke JL, Fliesler SJ, Darrow RM, Organisciak DT. Evidence for a circadian rhythm of light damage susceptibility in rats. Photochem Photobiol 2002;75:547–553. [PubMed: 12017483]
52. Vaughan DK, Coulibaly SF, Darrow RM, Organisciak DT. A morphometric study of light damage in transgenic rat models of retinitis pigmentosa. Invest Ophthalmol Vis Sci 2003;44:848–855. [PubMed: 12556421]
53. Xu L, Ball SL, Alexander KR, Peachey NS. Pharmacological analysis of the rat cone ERG. Vis Neurosci 2003;20:297–306. [PubMed: 14570251]
54. Dvornik D, Hill P. Effect of long-term administration of AY9944, an inhibitor of 7-dehydrocholesterol Δ7-reductase, on serum and tissue lipids in the rat. J Lipid Res 1968;9:587–595. [PubMed: 5726317]
55. Dvornik D, Kraml M, Dubuc J, Givner M, Gaudry R. A novel mode of inhibition of cholesterol biosynthesis [letter]. J Am Chem Soc 1963;85:3309.
56. Givner ML, Dvornik D. Agents affecting lipid metabolism, XV: biochemical studies with the cholesterol biosynthesis inhibitor AY-9944 in young and mature rats. Biochem Pharmacol 1965;14:611–619. [PubMed: 14322980]
57. LaVail MM. Outer segment disc shedding and phagocytosis in the outer retina. Trans Ophthalmol Soc U K 1983;103(pt 4):397–404. [PubMed: 6380008]
58. Nguyen-Legros J, Hicks D. Renewal of photoreceptor outer segments and their phagocytosis by the retinal pigment epithelium. Int Rev Cytol 2000;196:245–313. [PubMed: 10730217]
59. Fliesler SJ, Anderson RE. Chemistry and metabolism of lipids in the vertebrate retina. Prog Lipid Res 1983;22:79–131. [PubMed: 6348799]
60. Stubbs CD. Membrane fluidity: structure and dynamics of membrane lipids. Essays Biochem 1983;19:1–39. [PubMed: 6094185]
61. Yeagle PL. Cholesterol and the cell membrane. Biochim Biophys Acta 1985;822:267–287. [PubMed: 3904832]
62. Kofuji P, Ceelen P, Zahs KR, Surbeck LW, Lester HA, Newman EA. Genetic inactivation of an inwardly rectifying potassium channel (Kir4.1 subunit) in mice: phenotypic impact in retina. J Neurosci 2000;20:5733–5740. [PubMed: 10908613]
63. Hood DC, Birch DG. A computational model of the amplitude and implicit time of the b-wave of the human ERG. Vis Neurosci 1992;8:107–126. [PubMed: 1558823]

64. Fliesler, SJ. Effects of cholesterol biosynthesis inhibitors on retinal development, structure, and function. In: Fliesler, SJ., editor. Sterols and Oxysterols: Chemistry, Biology and Pathobiology. Kerala, India: Research Signpost; 2002. p. 77-109.
65. Boulton M, Rozanowska M, Rozanowski B. Retinal photodamage. J Photochem Photobiol. B 2001;64:144–161. [PubMed: 11744401]
66. Organisciak DT, Winkler BS. Retinal light damage: practical and theoretical considerations. Prog Ret Eye Res 1994;13:1–29.
67. Reme CE, Grimm C, Hafezi F, Iseli HP, Wenzel A. Why study rod cell death in retinal degenerations and how? Doc Ophthalmol 2003;106:25–29. [PubMed: 12675482]
68. Snodderly DM. Evidence for protection against age-related macular degeneration by carotenoids and antioxidant vitamins. Am J Clin Nutr 1995;62 1448S–1461S.
69. Winkler, BS.; Boulton, ME.; Gottsch, JD.; Sternberg, P. Oxidative damage and age-related macular degeneration [online serial]; Mol Vis. 1999 [Accessed March 22, 2004]. p. 32-42.Available at: http://www.molvis.org/molvis/v5/p32
70. Rao NA, Wu GS. Free radical mediated photoreceptor damage in uveitis. Prog Ret Eye Res 2000;19:41–68.
71. Vaughan, DK.; Richards, MJ.; Fliesler, SJ. DMTU protects against light-induced retinal degeneration in an animal model of Smith-Lemli-Opitz syndrome; Annual Meeting Abstract Search and Program Planner [book on CD-ROM]; Rockville, Md: Association for Research in Vision & Ophthalmology; 2002 Apr 1. Abstract 3729
72. Richards, MJ.; Nagel, BA.; Fliesler, SJ. Lipid hydroperoxide formation in an animal model of Smith-Lemli-Opitz syndrome: correlation with retinal degeneration and exposure to constant light; Annual Meeting Abstract Search and Program Planner [book on CD-ROM]; Rockville, Md: Association for Research in Vision & Ophthalmology; 2003 Apr 1. Abstract 3548
73. De Fabiani E, Caruso D, Cavaleri M, Galli Kienle M, Galli G. Cholesta-5,7,9(11)-trien-3β-ol found in plasma of patients with Smith-Lemli-Opitz syndrome indicates formation of sterol hydroperoxide. J Lipid Res 1996;37:2280–2287. [PubMed: 8978479]
74. Gaoua W, Chevy F, Roux C, Wolf C. Oxidized derivatives of 7-dehydrocholesterol induce growth retardation in cultured rat embryos: a model for antenatal growth retardation in the Smith-Lemli-Opitz syndrome. J Lipid Res 1999;40:456–463. [PubMed: 10064734]
75. Sakuragawa N, Sakuragaw M, Kuwabara T, Pentchev PG, Barranger JA, Brady RO. Niemann-Pick disease experimental model: sphingomyelinase reduction induced by AY-9944. Science 1977;196:317–319. [PubMed: 66749]
76. Yoshida Y, Arimoto K, Sato M, Sakuragawa N, Arima M, Satoyoshi E. Reduction of acid sphingomyelinase activity in human fibroblasts induced by AY-9944 and other cationic amphiphilic drugs. J Biochem (Tokyo) 1985;98:1669–1679. [PubMed: 2419314]
77. Igarashi M, Suzuki K, Chen SM. Changes in brain hydrolytic enzyme activities in rats treated with cholesterol biosynthesis inhibitor, AY9944. Brain Res 1975;90:97–114. [PubMed: 48406]
78. Irons M, Elias ER, Abuelo D, et al. Treatment of Smith-Lemli-Opitz syndrome: results of a multicenter trial. Am J Med Genet 1997;68:311–314. [PubMed: 9024565]
79. Linck LM, Lin DS, Flavell D, Connor WE, Steiner RD. Cholesterol supplementation with egg yolk increases plasma cholesterol and decreases plasma 7-dehydrocholesterol in Smith-Lemli-Opitz syndrome. Am J Med Genet 2000;93:360–365. [PubMed: 10951458]
80. Nwokoro NA, Mulvihill JJ. Cholesterol and bile acid replacement therapy in children and adults with Smith-Lemli-Opitz (SLO/RSH) syndrome. Am J Med Genet 1997;68:315–321. [PubMed: 9024566]
81. Starck L, Lovgren-Sandblom A, Bjorkhem I. Cholesterol treatment forever? the first Scandinavian trial of cholesterol supplementation in the cholesterol-synthesis defect Smith-Lemli-Opitz syndrome. J Intern Med 2002;252:314–321. [PubMed: 12366604]

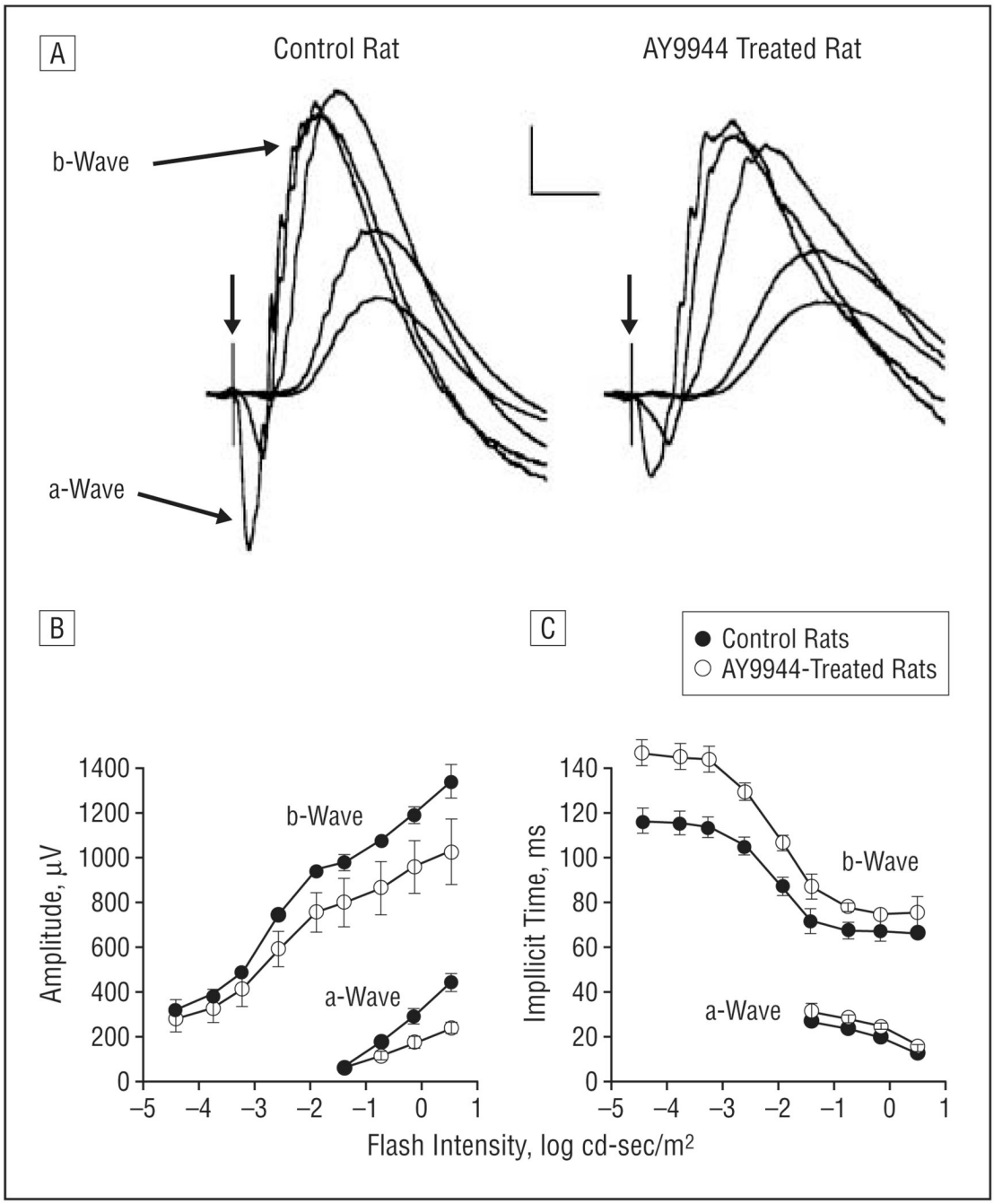

Figure 1.

Dark-adapted electroretinograms. A, Representative electroretinograms recorded from a control rat and a rat treated with AY9944 (*trans*-1,4-*bis* [2-dichlorobenzylamino-ethyl] cyclohexane dihydrochloride) to strobe flashes presented to the dark-adapted eye. Calibration indicates 200 μV and 50 milliseconds. In the flash intensity–response functions for a- and b-wave amplitudes (B) and implicit time (C), each point represents the mean value for 4 control rats and 5 rats treated with AY9944. Error bars represent SD; cd, candela.

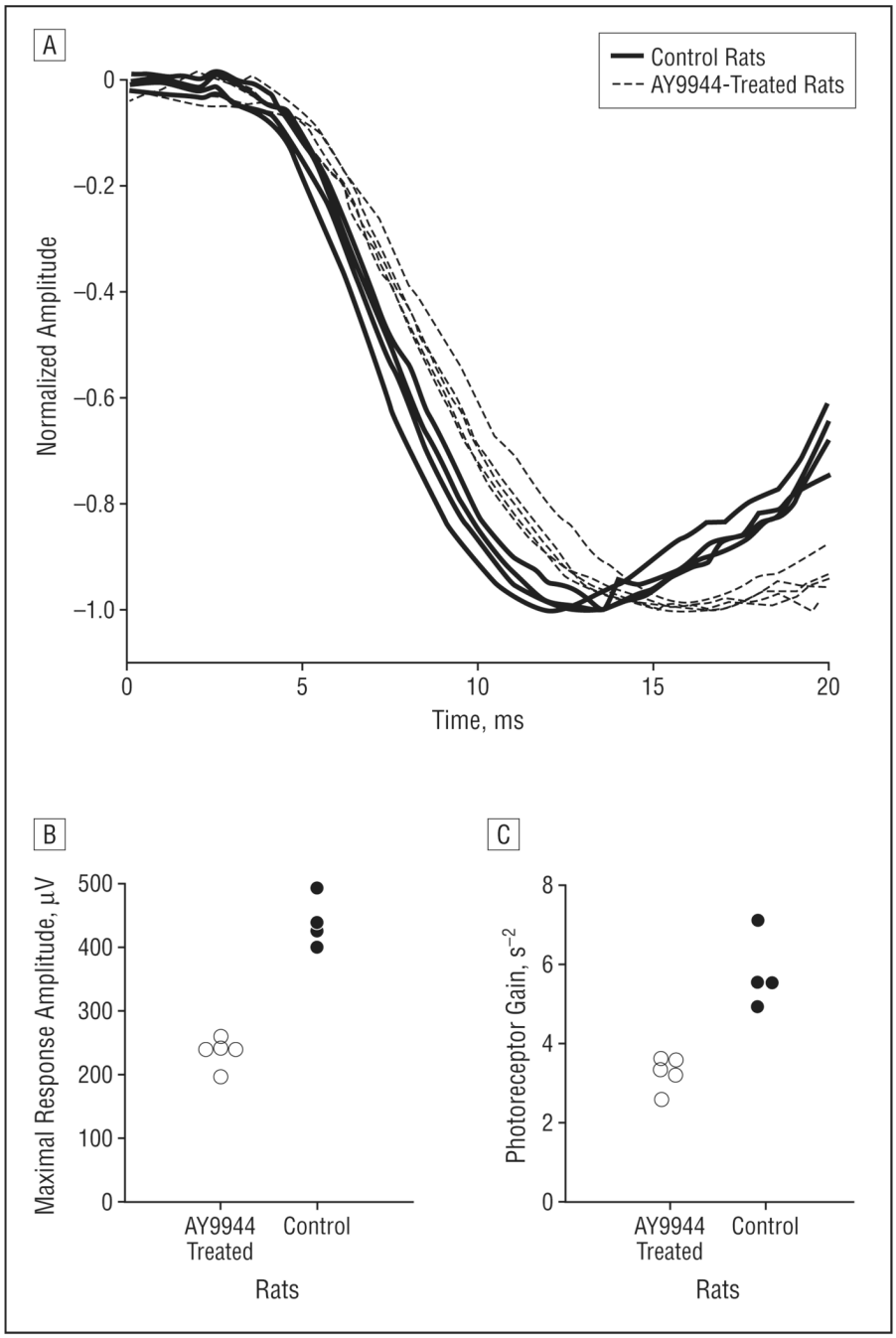

Figure 2.

Analysis of the leading edge of the rod electroretinographic a-wave. A, Initial portion of the rod electroretinogram obtained to a 0.5–log candela (cd)-sec/m^2 strobe flash, the highest flash intensity used in this study. Each waveform was obtained from a different rat, and each has been normalized by the maximal response amplitude. Distribution of values of is shown for maximal response amplitude (B) and photoreceptor gain (C) obtained for control rats and rats treated with AY9944 (*trans*-1,4-*bis* [2-dichlorobenzylamino-ethyl] cyclohexane dihydrochloride).

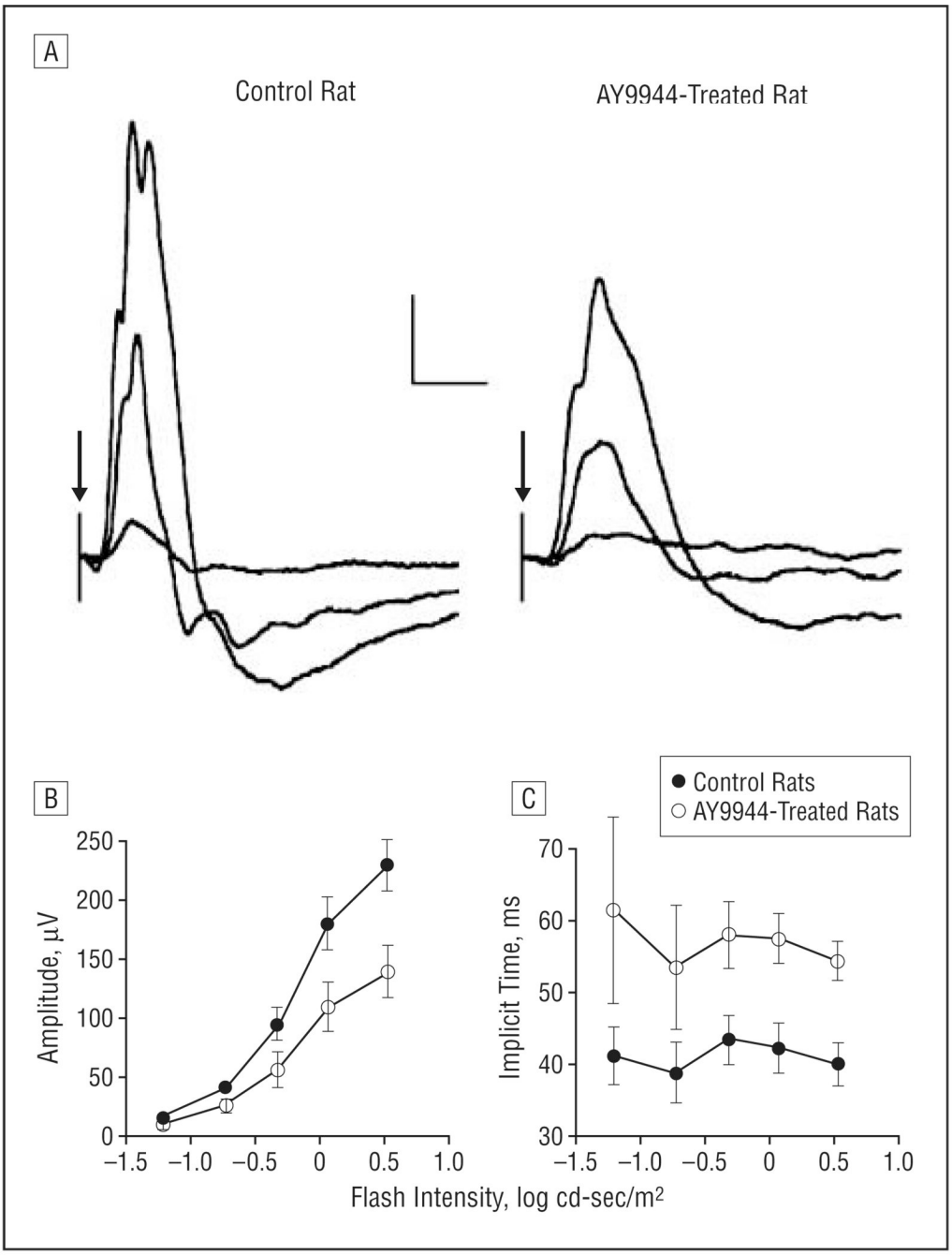

Figure 3.

Light-adapted electroretinograms. A, Representative cone electroretinograms recorded from a control rat and a rat treated with AY9944 (*trans*-1,4-*bis* [2-dichlorobenzylamino-ethyl] cyclohexane dihydrochloride) to strobe flashes superimposed on a steady rod-desensitizing adapting field. Calibration indicates 50 µV and 50 milliseconds. In flash intensity–response functions for cone amplitude (B) and implicit time (C), each point represents the mean value for 4 control rats and 5 rats treated with AY9944. Error bars represent SD; cd, candela.

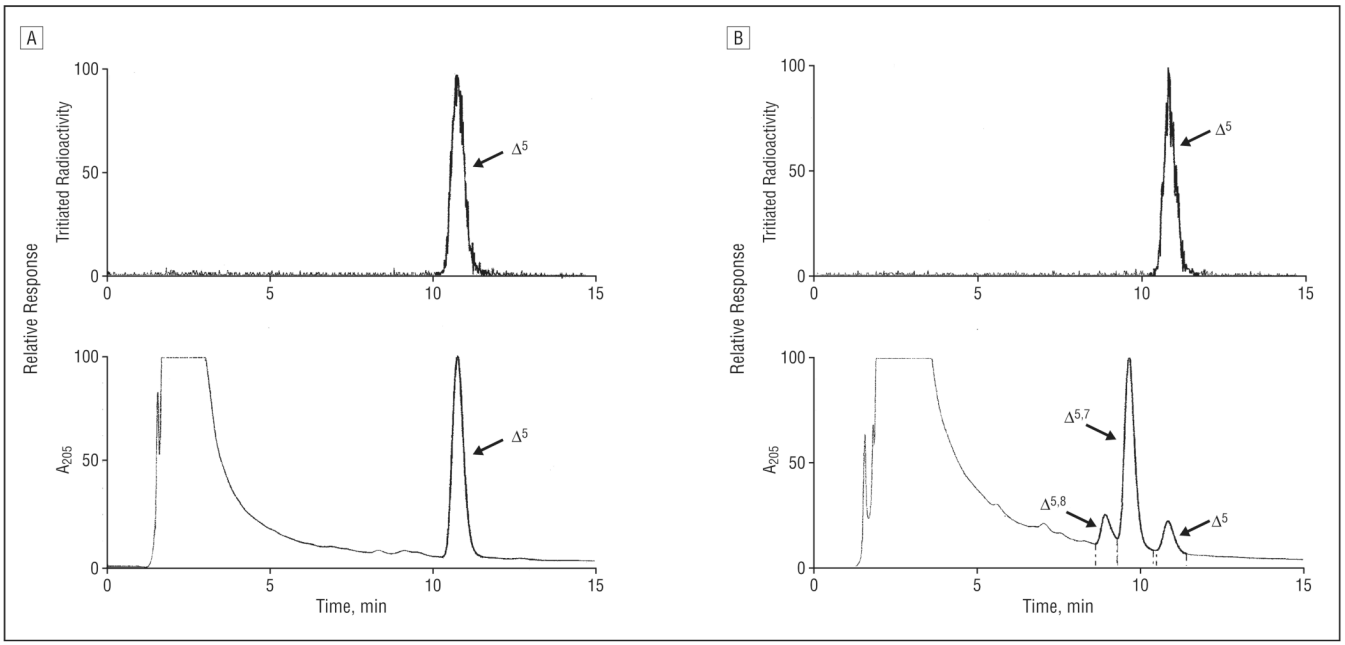

Figure 4.

Reverse-phase high-performance liquid chromatograms of nonsaponifiable lipid extracts from retinas of control rats (A) and AY9944 (*trans*-1,4-*bis* [2-dichlorobenzylamino-ethyl] cyclohexane dihydrochloride)-treated rats (B). The upper panels show the radioactivity detector response, demonstrating chromatographic elution of the [^{3}H] cholesterol internal standard; the lower panels, the UV detector response (absorbance at 205 nm). Elution positions of cholesterol (Δ5), 7-dehydrocholesterol (Δ5› 7), and 8-dehydrocholesterol (Δ5› 8) are indicated. Full-scale detector response is set for the maximum response of the dominant sterol component in each panel.

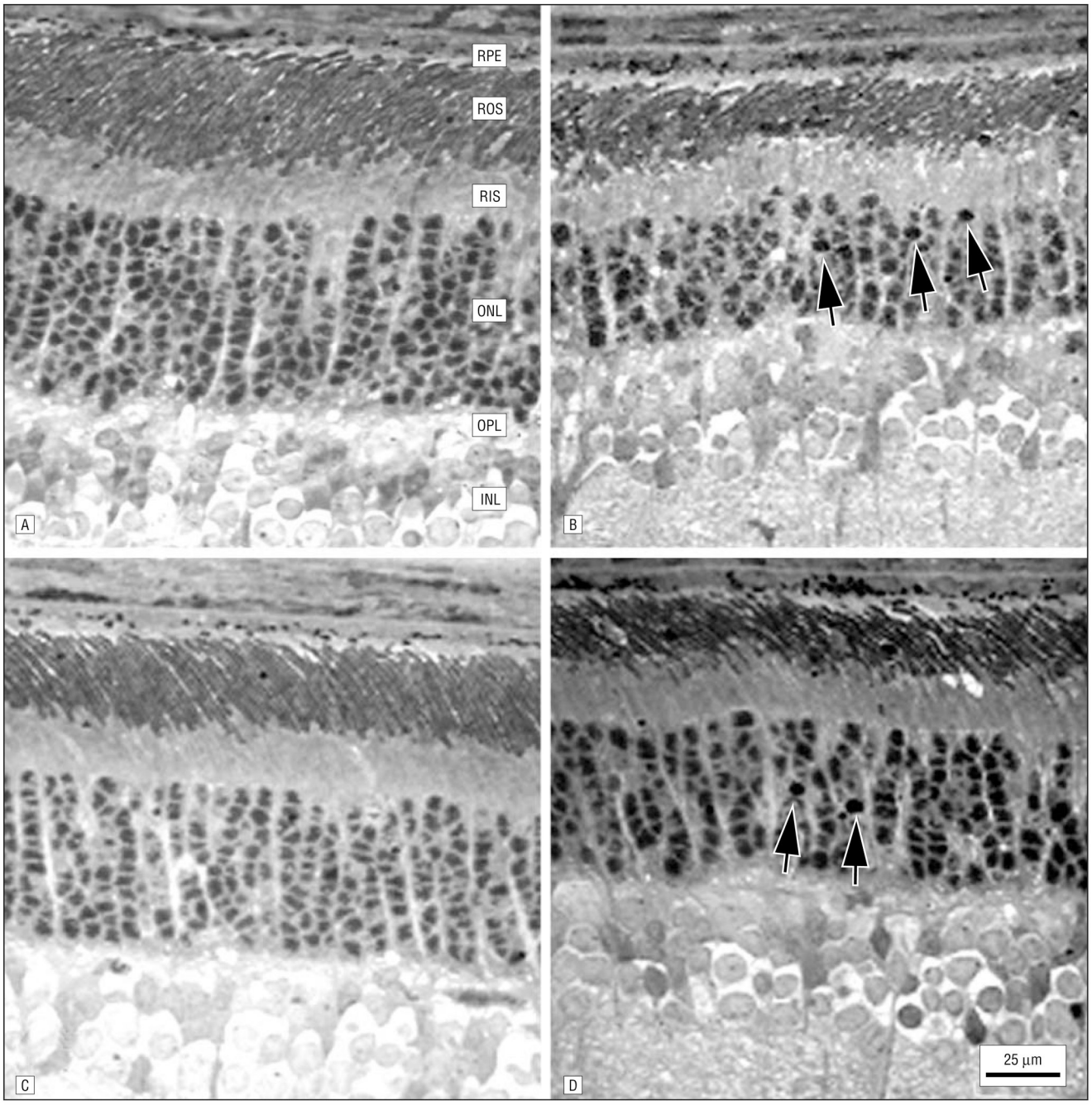

Figure 5.

Histologic changes in retinas from 3-month-old control (A and C) and AY9944 (*trans*-1,4-*bis* [2-dichlorobenzylamino-ethyl] cyclohexane dihydrochloride)-treated (B and D) rats corresponding to regions 2 mm from the optic nerve head in the superior (A and B) and inferior (C and D) hemispheres along the vertical meridian. Note the apparent reduction in outer nuclear layer (ONL) thickness and rod outer segment (ROS) length in the retinal regions of the AY9944-treated rat relative to the comparable regions of the control retina and the presence of pyknotic nuclei (arrows) in retinas of treated rats. RPE indicates retinal pigment epithelium; RIS, rod inner segment layer; OPL, outer plexiform layer; and INL, inner nuclear layer.

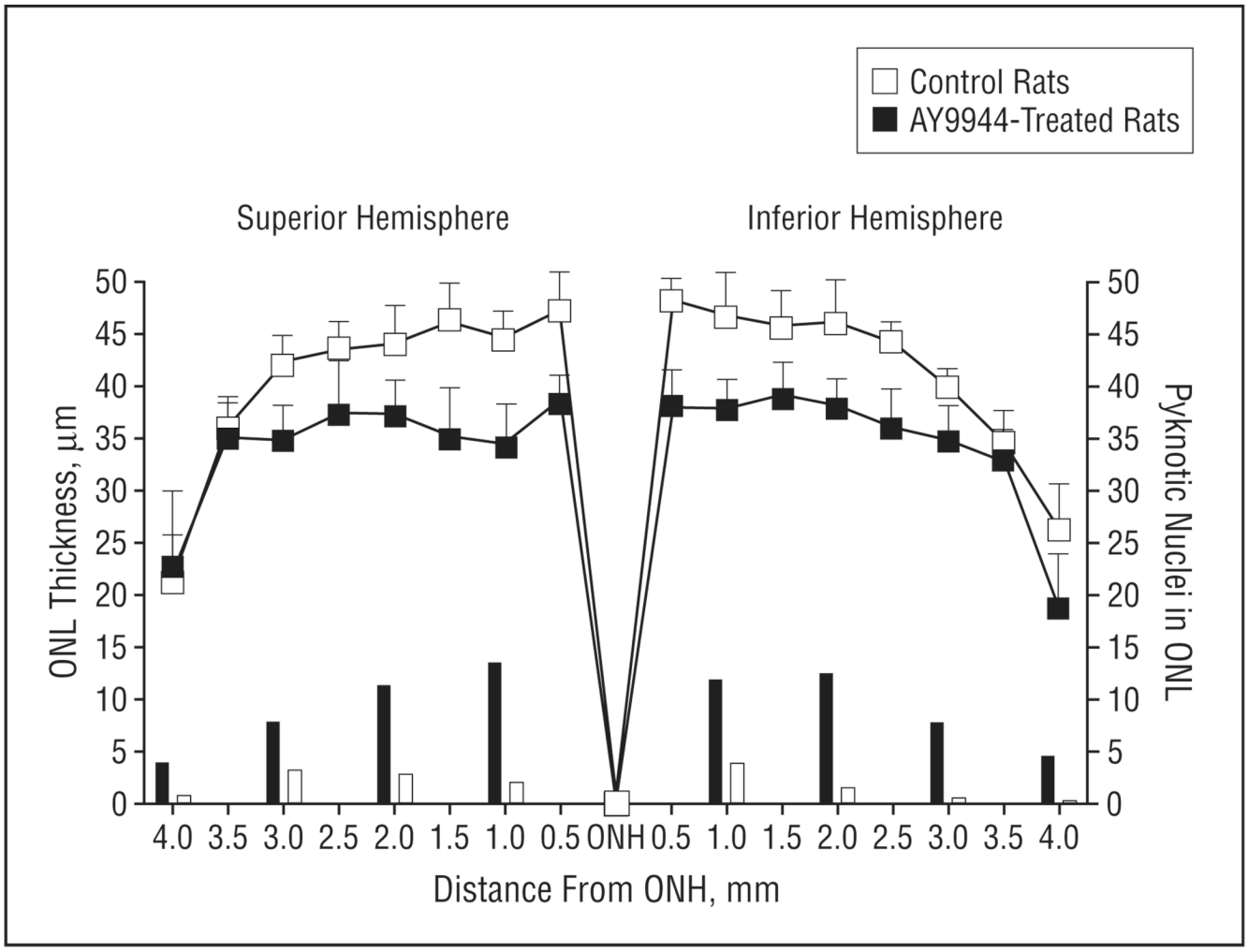

Figure 6.

Morphometric analysis of the outer nuclear layer (ONL) of retinas from control and AY9944 (*trans*-1,4-*bis* [2-dichlorobenzylamino-ethyl] cyclohexane dihydrochloride)-treated rats (aged 3 months). Mean ONL thickness values (plotted curves, 15 independent measurements per region) are measured at 0.5-mm intervals from the optic nerve head (ONH) along the vertical meridian. Mean pyknotic ONL nucleus counts (bar graphs) are given per 1-mm expanse along the vertical meridian. Error bars represent SD.

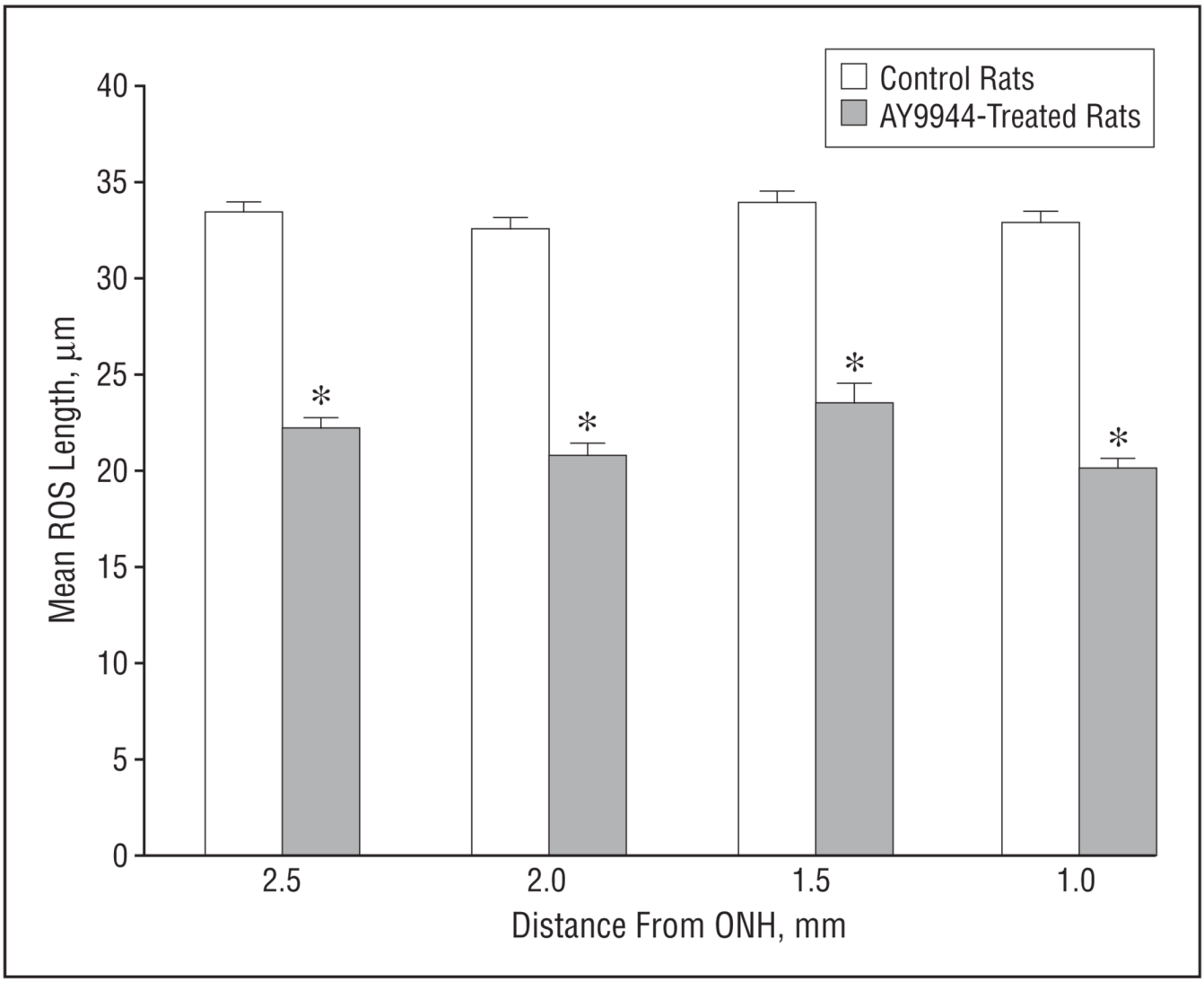

Figure 7.

Morphometric analysis of mean rod outer segment (ROS) length in retinas from control and AY9944 (*trans*-1,4-*bis* [2-dichlorobenzylaminoethyl] cyclohexane dihydrochloride)-treated rats. Measurements (N=30) were taken in the superior retinal hemisphere at 0.5-mm intervals along the vertical meridian, 1.0 to 2.5 mm from the optic nerve head (ONH). Asterisk ndicates a statistically significant difference in ROS length measurements in control vs treated retinas at each retinal region examined ($P<.001$). Error bars represent SD.

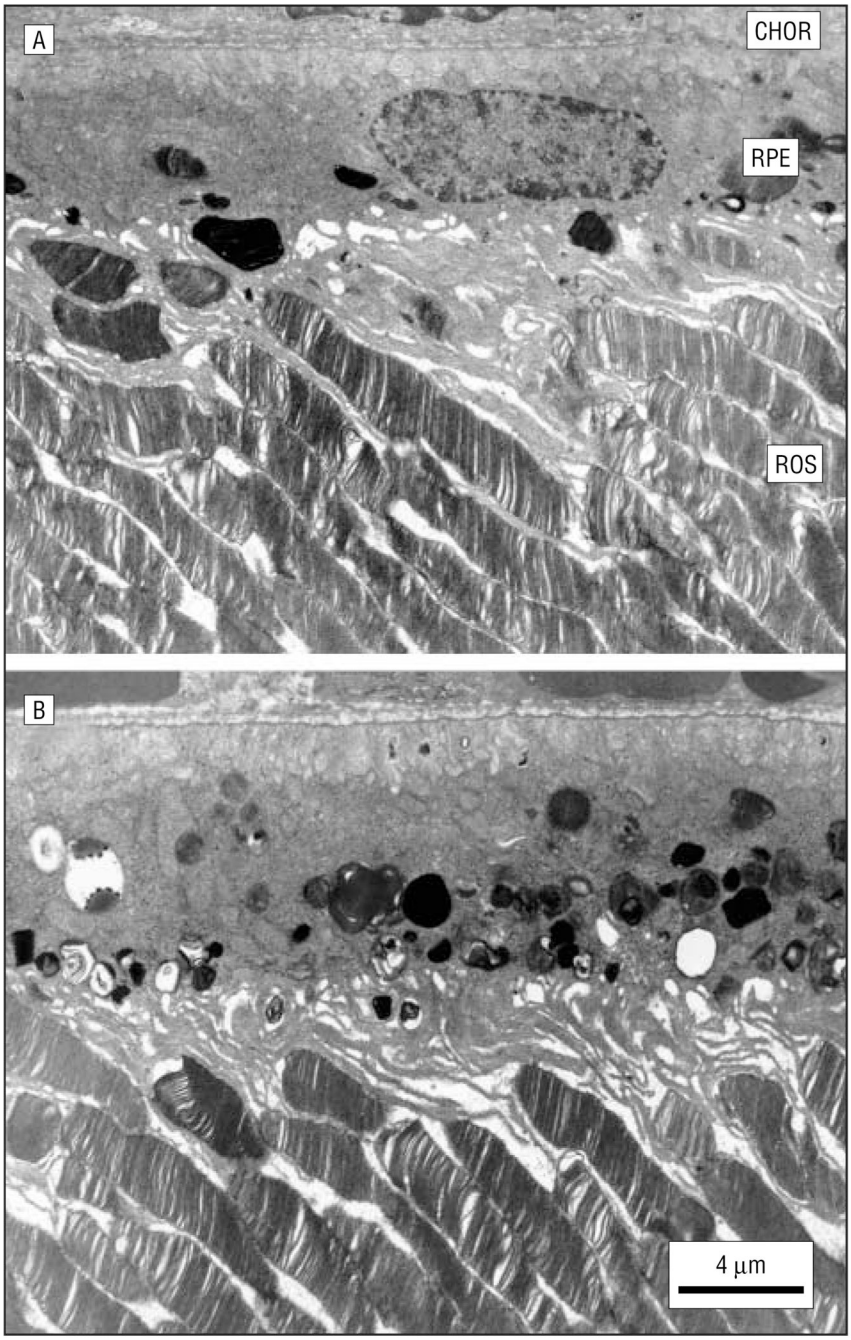

Figure 8.
Ultrastructure of the retina and underlying retinal pigment epithelium (RPE)–choroid (CHOR) in a 3-month-old control rat (A) and an age-matched AY9944 (*trans*-1,4-*bis* [2-dichlorobenzylamino-ethyl] cyclohexane dihydrochloride)-treated rat (B). Note the marked accumulation of membranous and lipid inclusions in the RPE of the treated rat eye. ROS indicates rod outer segment.

Table

Sterol Composition of Retina and Serum From AY9944-Treated and Control Rats*

	Retina		Serum	
Rat	7DHC/Chol†	Total Sterol, nmol/retina	7DHC/Chol†	Total Sterol, mg/dL
AY9944 treated	5.30 ± 1.7	51.2 ± 5.1	8.68 ± 0.95	21.9 ± 1.8
Control	ND‡	64.0 ± 2.6	ND	87.1 ± 6.6

Abbreviations: Chol, cholesterol; 7DHC, 7-dehydrocholesterol; ND, not detected.

*Values (mean ± SD, N = 5) were determined by reverse-phase high-performance liquid chromatographic analysis of extracted nonsaponifiable lipids, corrected for recovery efficiency using an internal standard of tritiated cholesterol.

†Mole ratio of 7DHC to cholesterol; the sum of these sterols is 90% or greater of the total sterols detected.

‡The 7DHC level is below the level of detection; hence the 7DHC/Chol ratio is approximately zero.